ADVANCED FUNCTIONAL MATERIALS
www.afm-journal.de

Extrusion Printing of Flexible Electrically Conducting Carbon Nanotube Networks

*Geoffrey C. Pidcock and Marc in het Panhuis**

Carbon nanotube networks in biopolymer solutions are explored as potential ink systems for the extrusion printing of conducting structures. The biopolymer gellan gum is found to act as an excellent dispersant of multiwalled carbon nanotubes and has the appropriate flow properties to act as a thickener for the controlled dispensing of carbon nanotube networks. Absorbing substrates are found to improve the resolution and the flexibility of the printed structures. These printed conducting carbon nanotube networks exhibit interesting mechanical and electrical characteristics, which are applied to demonstrate their actuating and strain gauging capabilities.

1. Introduction

Printing is the deposition of a material (ink) onto a substrate in order to produce a desired structure. Specialist technologies are increasingly requiring advanced materials properties from the printed structures, such as flexible, stretchable conductors and sensors.[1–3] There is a drive to develop new printing processes to further extend the sophistication and the capabilities of the printed structures. Extrusion printing (also known as direct writing and solid free-form fabrication) is a process that involves the pressurized delivery of an ink through a capillary onto a moving substrate.[4,5] Relative to other printing processes, extrusion printing offers greater flexibility in the ink materials and a large range in the printed structure's minimum feature sizes (or resolution); from the micro to the macroscale.[6] Extrusion printing can also manufacture three dimensional, structurally robust structures, and embed material into substrates.[7] This functionality makes up for some of the draw-backs (e.g., resolution) compared to other methods such as inkjet printing.[7–9]

Carbon nanotubes (NTs) are carbon allotropes that display high aspect ratios and surface areas as well as excellent thermal, electrical, and mechanical properties.[10–12] Their industrial scale production involves processes such as chemical vapour deposition, which, whilst economical, result in large variations of both geometry and chemical composition.[13] The impact of these heterogeneities to bulk properties can be largely mitigated through the ensemble averaging of large amounts of nanotubes found in macroscopic networks.[14] Carbon nanotube networks (NNs) are clusters of randomly positioned and randomly aligned carbon nanotubes with consistent connections found over large length scales.[15,16] The formation of a NN within a matrix material can impart significant changes to the composite flow and electrical properties.[16–18] NN formation is often modelled using "statistical percolation theory", whereby properties that are dependent upon nanotube connections, such as the conductivity, scale with loading from a critical threshold in a manner proportional to the network's dimensionality.[15,16]

Printing of high resolution NN-polymer composites requires the dispersion of NTs into the polymer matrix so that the network is homogenous–and more practically, so that the extruding capillary does not clog. It has been estimated that particles should be kept below 1/100 of the capillary radius to prevent clogging, placing a strong requirement for well dispersed nanotube ink systems in high resolution printing.[5] The high surface area of NTs introduces a significant barrier to dispersion, as van der Waals forces act to agglomerate the NTs into bundles (with an estimated interaction energy of 500 eV/μm).[19] This interaction can be reduced through the non-covalent modification of the nanotube surface using a variety of surfactants and polymers.[20–23] When coupled with high energy (such as sonolysis) to break apart the nanotube bundles, NTs can be dispersed into an aqueous solution.[21,24,25] 'Non-covalent solution processing' is not without its problems: there is strong evidence that excessive energy during dispersion degrades the nanotubes, and popular surfactants such as sodium dodecyl sulfate (SDS) place significant limitations upon the dispersed NT concentration.[26,27] The goal of printing is therefore tied to the goal of producing completely dispersed NT at low energy deliveries and at high concentrations.

Gellan gum (GG) is a linear, anionic polysaccharide produced by *Sphingomonas elodea*.[28] The commercial product consists of deacylated tetrasaccharide repeat units of β-D-glucuronic acid and α-L-rhamnose alternating with β-D-glycose. Gellan gum is USA FDA and European Union (E418) approved for food and medical usage, and has found wide application as a multifunctional gelling, stabilising and suspending agent. It also has interesting rheological properties which imply that it is effective as a thickener to achieve the appropriate window of viscosity for extrusion printing.[29]

G. C. Pidcock, Prof. M. in het Panhuis
Soft Materials Group
School of Chemistry
University of Wollongong
Wollongong, NSW 2522, Australia
E-mail: panhuis@uow.edu.au
Prof. M. in het Panhuis
ARC Centre of Excellence for Electromaterials Science
University of Wollongong
Wollongong, NSW 2522, Australia

DOI: 10.1002/adfm.201200724

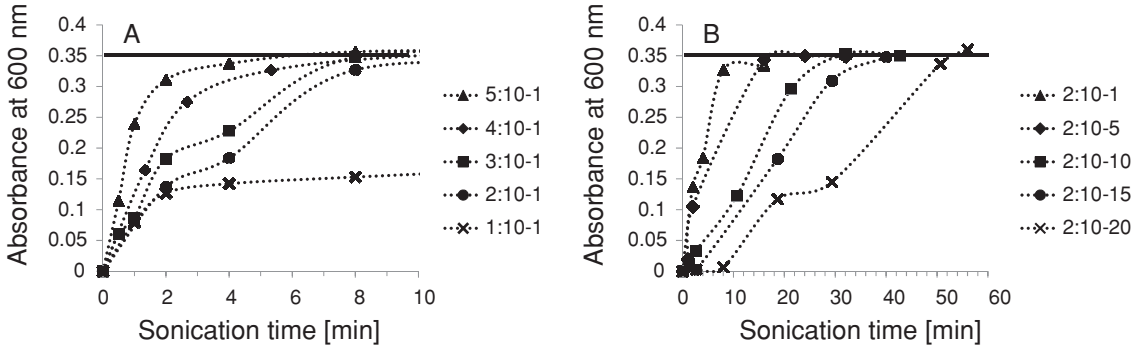

Figure 1. a) UV-vis absorbance (at 600 nm) as a function of sonication time (at 6 °C), at 1 mg/mL initial MWNT (diluted 1/150) and for a variety of GG:MWNT ratios. The solid line indicates the expected absorbance for a complete dispersion. b) UV-vis absorbance (at 600 nm) vs. time for the 2:10 GG:MWNT system as a function of MWNT concentration at 6 °C. The solid line indicates the expected absorbance for a complete dispersion. The naming convention in legend is as follows, (ratio GG:MWNT)-MWNT concentration, e.g., "2:10-15" indicates a dispersion with GG:MWNT ratio of 2:10 and GG and MWNT concentrations of 3 mg mL^{-1} and 15 mg mL^{-1}, respectively.

Here, a gellan gum–carbon nanotube ink system for extrusion printing conducting carbon nanotube networks is investigated. The GG-MWNT dispersion is optimized in terms of minimum ratio between conducting filler and dispersant. We show that gellan gum can deliver the necessary window of ink flow properties required for extrusion printing the optimized inks. Printed carbon nanotube networks exhibited interesting electrical and mechanical characteristics. It is demonstrated that these printed structures display actuating and strain gauging capabilities.

2. Results and Discussion

2.1. Optimization of Gellan Gum–Carbon Nanotube Dispersions

Previous studies have shown a strong correlation between UV-vis absorbance intensity and dispersed MWNT.[27] As such, the ability of gellan gum to disperse NTs was determined by monitoring the leveling of the UV-vis absorbance intensity and disappearance of visible aggregates. Figure S1a (Supporting Information) shows that a MWNT dispersion (MWNT concentration 1 mg/mL, GG:MWNT ratio 5:1) can be assumed to have reached completion after 8 min. This sonication time is equivalent to a total energy input of 2.88 kJ (or 320 J per mg of dispersed MWNT). The resulting MWNT extinction coefficient of (5.14 ± 0.09) x 10^{-2} L mg^{-1} cm^{-1} from the standard curve (Figure S1b, Supporting Information) is in good agreement with spectral data published for surfactant-dispersed MWNTs produced by the same supplier (Nanocyl S. A., Belgium).[27]

The GG:MWNT dispersion system was then optimized by evaluating the following performance parameters: i) minimum viable ratio (r_{min}), the lowest GG:MWNT ratio that results in a complete dispersion, i.e., where the UV-vis absorbance intensity reaches the maximum value as predicted by the extinction coefficient; ii) scalability (s), the maximum MWNT concentration that can be completely dispersed at the minimum viable ratio; iii) expense ($E_\$$), the minimum energy required to completely disperse a given mass of carbon nanotubes; and iv) stability, the change in MWNT UV-vis absorbance intensity over 2 months.

GG was found to completely disperse 1 mg mL^{-1} MWNTs through a number of dispersant ratios ranging from 5:10 to 2:10 GG:MWNT, while the 1:10 GG:MWNT dispersion was found to asymptote in absorption below completion (**Figure 1**a). As such, the r_{min} for GG-MWNT dispersions lies between 2:10 and 1:10 GG:MWNT. The expense (**Table 1**) was found to increase linearly with decreasing GG concentration in the 1 mg mL^{-1} MWNT dispersions to $E_\$ = 810 \pm 20$ J mg^{-1} at r_{min} = 2:10 GG:MWNT. The GG-MWNT system at the minimum viable GG:MWNT ratio (2:10) was found to scale to at least s = 20 mg mL^{-1} (Figure 1b). The expense decreased with increasing MWNT loading, to $E_\$ = 110 \pm 10$ J mg^{-1} at s = 20 mg mL^{-1} concentration (Table 1).

The change in absorbance over 60 days following preparation (under standard temperatures and pressures) was found to be negligible for both 5:10 and 2:10 GG:MWNT dispersions; implying that all completed GG:MWNT dispersions at 1 mg mL^{-1} MWNT were stable for at least 2 months (Figure S2, Supporting Information). When the 2:10 system was scaled above

Table 1. Summary of expense ($E_\$$) values obtained from the UV-vis absorbance data shown in Figure 1. Naming convention for the dispersions is as follows, (ratio GG:MWNT)-MWNT concentration, e.g., "2:10-15" indicates a dispersion with GG:MWNT ratio of 2:10 and GG (c_{GG}) and (c_{MWNT}) MWNT concentrations of 3 mg mL^{-1} and 15 mg mL^{-1}, respectively.

Dispersion	c_{GG} [mg mL^{-1}]	c_{MWNT} [mg mL^{-1}]	$E_\$$ [J mg^{-1}]
1:10-1	0.1	1	–
2:10-1	0.2	1	810 ± 20
3:10-1	0.3	1	650 ± 50
4:10-1	0.4	1	387 ± 7
5:10-1	0.5	1	240 ± 20
2:10-5	1	5	182 ± 6
2:10-10	2	10	120 ± 10
2:10-15	3	15	110 ± 10
2:10-20	4	20	110 ± 10

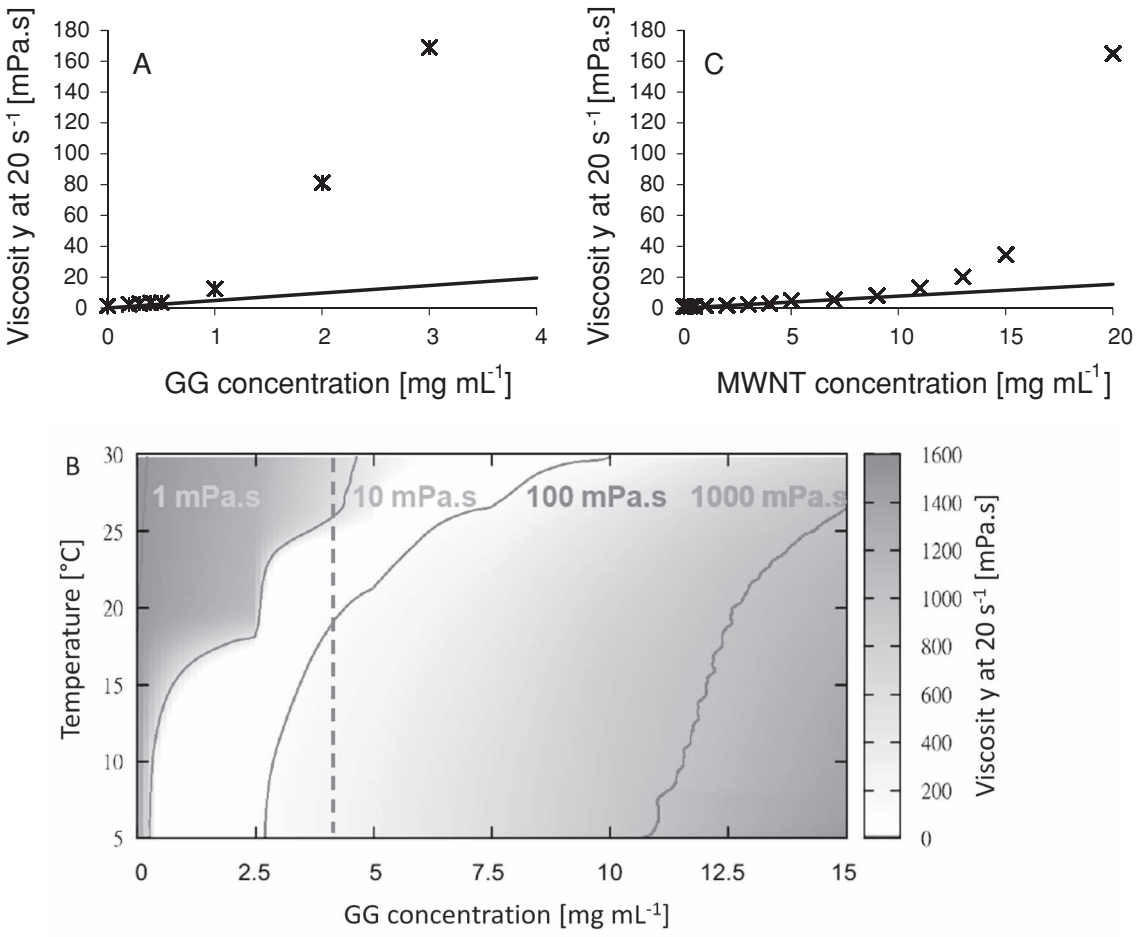

Figure 2. a) Viscosity (at shear rate = 20 s^{-1}) of GG solutions as a function of GG concentration at 5°C. b) The GG viscosity map, with viscosity (at shear rate = 20 s^{-1}) plotted in false color as a function of both concentration and temperature. Note: the contour kinks and the inconsistency with the grey scale are a consequence of data smoothing. The dashed line represents the maximum GG concentration used to disperse MWNTs in this paper (4 mg mL^{-1} GG, for 2:10-20). c) Viscosity (at shear rate = 20 s^{-1}) of GG:MWNT dispersions as a function of MWNT concentration, at a GG:MWNT ratio of 2:10. Straight lines in (a) and (c) are fits to viscosity at the lower concentrations.

a MWNT concentration of 15 mg mL^{-1}, a shorter period of stability (days) followed by a gradual decrease in the dispersed phase concentration was observed. This shorter period of stability is not a significant issue, as most solution processing methods such as fiber spinning, and printing require a dispersion stability period of less than 24 h.

These performance measures were benchmarked to data published for sodium dodecyl sulphate–a popular surfactant used in NT solution processing.[23,27] Analysis of the data for the SDS:MWNT system described in ref. [27] yielded r_{min} = 3:2, s = 14 mg mL^{-1} at $E_{\$}$ = 770 J mg^{-1}. This suggests that GG can disperse NTs with less expense, at lower dispersant:MWNT ratios and higher MWNT loading compared to SDS. It is well-known that SDS's ability to disperse is limited by self-association.[27,30] Gellan gum's ability is not without limitations, as explored below.

Carbon nanotube solution processing relies upon establishing a favourable balance between the rates of dispersant adsorption and desorption; these rates in turn relate to the mobility and availability of the dispersant, and the dispersant-nanotube binding energy.[31] Polymer solutions of GG in the absence of ions undergo two critical transitions–from dilute to semi-dilute, and from liquid/solution phase (sol) to gel phase.[32] These transitions are relevant to nanotube solution processing, as the first is followed by exponentially increasing matrix viscosity, which drives down the dispersant mobility; and the second radically reduces the availability of free gellan gum chains.

Viscosity measurements (**Figure 2**a) were used to construct a gellan gum viscosity map (Figure 2b) showing the dilute to semidilute transition indicated approximately by the 10 mPa.s contour. Thus, increasing the MWNT concentration in the dispersions (with r_{min} = 2:10 and temperature during sonolysis of 6 °C) above 5 mg mL^{-1} results in a GG concentration in the semi-dilute regime. The resulting increase in the dispersant viscosity (Figure 2a) only provides a partial explanation for the increase in time required to completely disperse MWNT at concentration >5 mg mL^{-1} MWNT (Figure 1d).

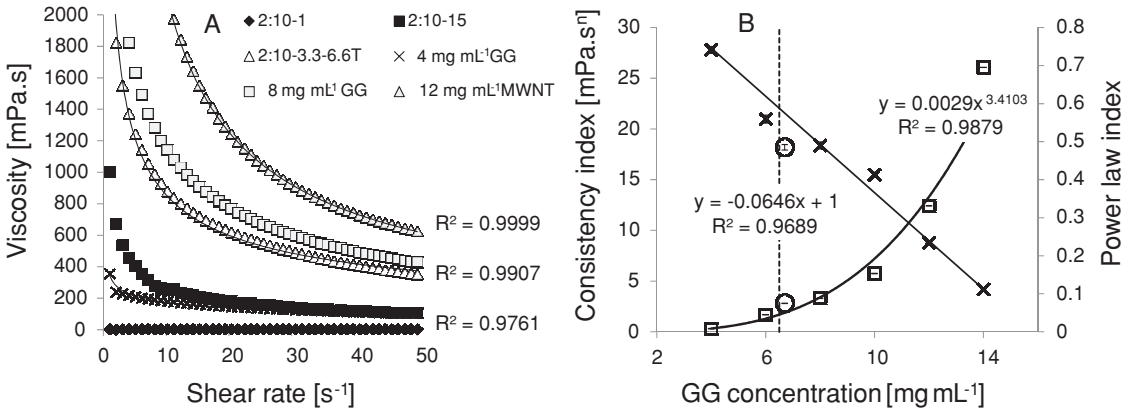

Figure 3. a) Viscosity at 19 °C as a function of shear rate in MWNT dispersions (below (2:10-1) and above (2:10-15) the semidilute transition, GG solutions (4, 8, and 12 mg mL^{-1}) and a GG thickened dispersion (3.3 mg mL^{-1} MWNT, 6.67 mg mL^{-1} unsonicated GG: 2:10-3.3-6.6T). The lines are fits to Equation 1. b) Consistency index (*K*) and power-law index (*n*) as a function of GG concentration. Solid lines are power-law and linear fits to *K* and *n* data, respectively. The dotted line indicates the minimum GG concentration required to achieve the target flow rate. The *K* and *n* values of the NTI ink are indicated by the circles.

The MWNT also undergo a dilute to semi-dilute transition, which is hereafter referred to as the rheological percolation.[18] Monitoring the viscosity of complete dispersions at r_{min} = 2:10 GG:MWNT showed rheological percolation occurs at 10 mg mL^{-1} (Figure 2c). This viscosity transition may provide a more fundamental limit to the dispersion rate, as it is caused by nanotube aspect ratio and cannot be reduced through sonication scission as readily as the GG viscosity.[18,26,33]

2.2. Ink Formulation

GG:MWNT dispersions below the MWNT dilute to semi-dilute transition have only a slightly higher viscosity (η) than water (~1 mPa.s, **Figure 3**a), due to the dispersant molecular weight being radically reduced by the sonication process.[34–36] Dispersions therefore need to be thickened to be appropriate for extrusion printing. The addition of small concentrations of unsonicated gellan gum (above its dilute to semidilute transition) was found to thicken the inks (Figure 3a), and impart pseudoplastic (non-Newtonian) flow behavior. The resulting flow curves are commonly modelled using the power-law model:

$$\eta = K\dot{\gamma}^{n-1} \quad (1)$$

where $\dot{\gamma}$ is the shear rate, *K* is the consistency index, and *n* is the power law index.[37] In a polymer-solution (such as GG), the solution becomes thinner under higher shear rates, resulting in a power law index that is less than one.[29] The viscosities of semi-dilute GG concentrations were measured as a function of shear rate, producing a series of power law parameters (Figure 3b). As the GG concentration increased, the solutions were found to become more shear thinning (*n* decreases), and much thicker (*K* increases). The shear thinning exponent and consistency index were found to be linearly and exponentially proportional to GG concentration, respectively (Figure 3b).

Provided the nanotubes are used well below their rheological percolation (~10 mg mL^{-1}, Figure 2c), it was assumed that the bulk flow properties will be dominated by the thickener GG concentration. The consistency index required for printing structures at our target resolution (line width below 300 μm) through a 50 μm capillary at flow rate of 40 μL/min was estimated at 1.72 $Pa.s^n$ (see Supporting Information). The GG concentration-consistency index fit (Figure 3b) was used to estimate the minimum thickening GG concentration as 6.5 mg mL^{-1}. As such, nanotube inks (NTI) were composed of 3.3 mg mL^{-1} MWNT (MWNT:GG 2:10) and 6.67 mg mL^{-1} thickener GG. The resulting ink exhibited consistency index and power law index values of 0.30 ± 0.03 $Pa.s^{0.515}$ and 0.485 ± 0.007, respectively.

2.3. Ink Properties

A series of inks thickened with 6.67 mg mL^{-1} GG were prepared with different MWNT concentrations using a 20 mg mL^{-1} MWNT dispersion, which were cast and evaporated into free-standing films under controlled ambient conditions. Thermogravimetric analysis (Figure S3, Supporting Information) showed a two-step decomposition pattern characteristic of GG, release of water molecules (<100 °C) and decomposition of the GG chain structure (220–320 °C).[38,39] The MWNT mass (M_f) and volume (V_f) fractions were calculated from each ink's nanotube and thickener GG concentrations and the MWNT and GG densities, i.e. 2.15 g cm^{-1} and (1.30 ± 0.03) g cm^{-1}, respectively.[40] The scaling of the conductivity (σ) with MWNT mass fraction (**Figure 4**a) was fitted to the statistical percolation model:

$$\sigma = \sigma_0 \left(M_f - M_{fp}\right)^t \quad (2)$$

where σ_o is a conductivity scaling factor, M_{fp} is the percolation threshold, and *t* is the conductivity exponent. The percolation

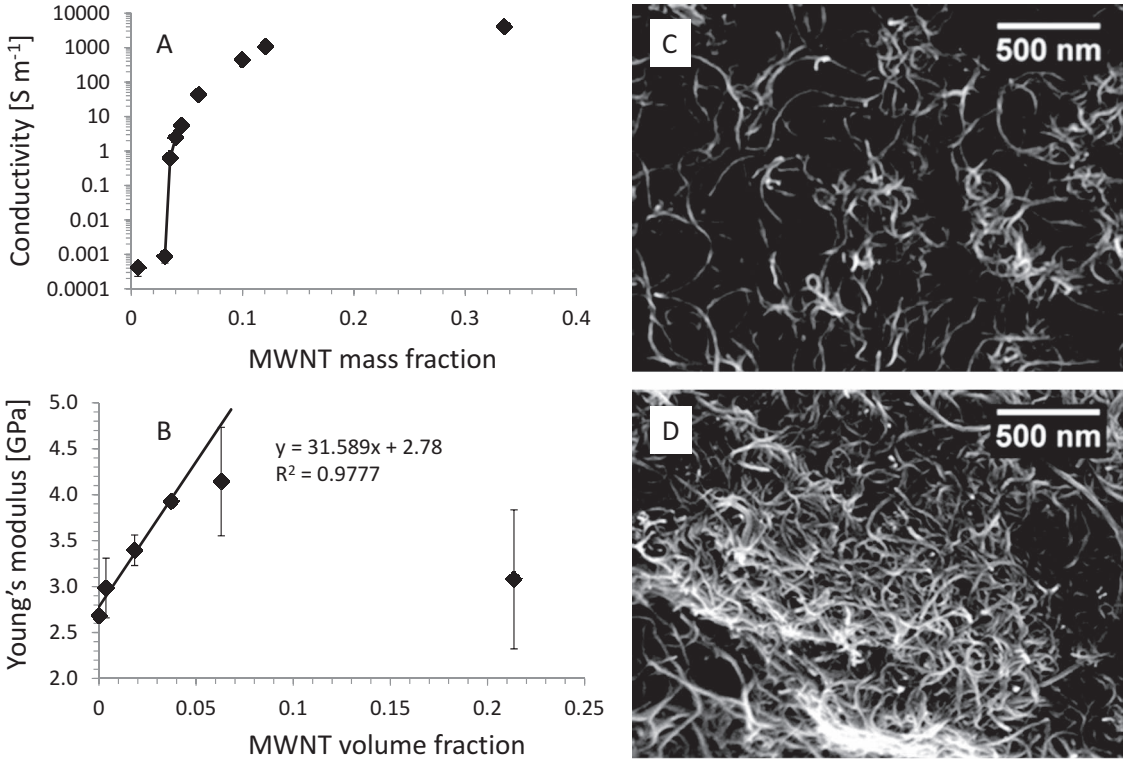

Figure 4. a) The scaling of conductivity with MWNT mass fraction (M_f), with error bars representing one confidence interval either side of the data point (95%, n = 4). The solid line is the three-parameter fit of the conductivity (between $M_f = 0.0302$ and $M_f = 0.0450$) to the statistical percolation model (Equation 2), sum of square residuals value = 1×10^{-7}. b) Scaling of Young's modulus as a function of the MWNT volume fraction (V_f). Error bars represent one standard deviation either side from the mean (n = 3). Straight line is a linear fit in MWNT volume fraction range 0 to 0.037. c,d) SEM images of films with $M_f = 0.06$ ($V_f = 0.037$) and $M_f = 0.33$ ($V_f = 0.23$), respectively.

threshold, at M_{fp} = 0.030 (V_{fp} = 0.018) is comparable to the thresholds observed in other (CVD) MWNT-polymer systems.[16] The conductivity exponent (t = 1.97) is in good agreement with the calculated value for a 3D percolative system (t = 2.0).[15,16]

The conductivity increased with CNT mass fraction towards the maximum possible conductivity of 5030 ± 50 S m^{-1} (M_f = 0.80) for this system. The maximum conductivity was found to be the same as other high loading CVD-MWNT-polymer composites and comparable to CVD-MWNT bucky-papers (1800–6000 S m^{-1}).[16,36]

The interaction between the matrix (GG) and the filler (MWNT) can be gauged through measuring the composite elastic (Young's) modulus (E), relative to the MWNT volume fraction (dE/dV_f), Figure 4b.[41] GG was found to be a brittle, glassy polymer matrix. Addition of nanotubes was found to degrade the mechanical properties at high loadings. Specifically, the extensibility was markedly reduced (to an average value of 1.5% tensile strain), and the modulus and the strength were found to increase to a maximum (around V_f = 0.06), and then decrease at high volume fractions. The initial increase in the modulus with the volume fraction was found to be linear, and provides an estimate of the GG-MWNT dE/dV_f of 32 ± 3 GPa. This estimate suggests that there is some interaction between the filler and the matrix, of comparable magnitude to solution cast CVD-MWNT's in polyethylene (dE/dV_f = 30 GPa).[38]

2.4. Extrusion Printing

MWNT-GG lines were deposited (at 40 nL mm^{-1}) on glass, photo-paper, LDPE, and plasticized GG (GGp) and CH (CHp) substrates (**Figure 5**a). The low surface energy of the absorbing GGp (ink-substrate contact angle, θ = 91 ± 3°) and CHp (θ = 106 ± 2°) substrates enabled them to share the advantages of photo-paper (θ = 124.9 ± 0.1°), in that the surface minimises the contact area, but the capillary absorbing bulk provides the necessary adhesion to stabilise the printed line (filament), Figure S4 (Supporting Information).

The electrical and mechanical characteristics of conducting tracks deposited on the flexible absorbing substrates GGp and CHp were compared to a non-absorbing LDPE substrate (θ = 65 ± 1°). Profilometry and optical microscopy of the cross-sections revealed that on LDPE (where no substrate absorption took place) the ink dried to a film of width (w) = 595 ± 39 μm and cross-sectional area (A_{cross}) = 345 ± 13 μm^2. Whereas on GGp the ink was mostly embedded as is evident from its decrease in width (327 ± 12 μm) and increase in cross-sectional area (8665 ± 1605 μm^2) compared to the ink on LDPE. The ink deposited on the CHp substrates was found to display very different absorption behavior. The ink formed a surface conducting structure (dimensions of w = 237 ± 7 μm, A_{cross} = 2762 ± 62 μm^2), which was partially embedded within the substrate. Regardless, the effect is the same for printing onto CHp and GGp, ink interacting with absorbing substrates.

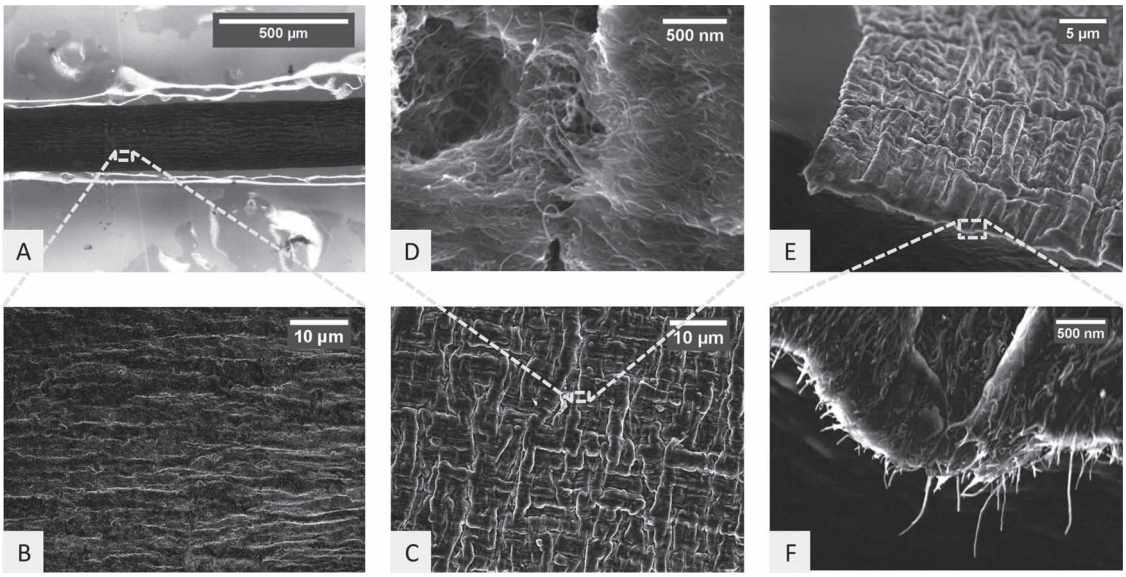

Figure 5. a) Optical and b) SEM images of the surface of a NTI line (1 layer) printed onto a CHp substrate. c–f) SEM images of the surface morphology of a NTI line (1 layer) printed onto a CHp imaged after straining to failure (~70% strain, at 1% strain s^{-1}): c) the surface of the printed line after straining to failure, d) a close-up of a surface crack, e) the fracture surface, and f) enlarged view of image shown in (e).

The measured resistance of printed tracks (length 1 cm, one layer) was found to differ significantly between the substrates. A single track on LDPE resulted in a sample resistance of 15 ± 1 kΩ cm^{-1} (conductivity, σ = 1914 ± 172 S m^{-1}) whereas tracks on absorbing substrates yielded higher resistance (lower conductivity) values due to ink-substrate interactions, i.e., 30 ± 10 kΩ cm^{-1} (σ = 107 ± 23 S m^{-1}) for CHp, and 46 ± 9 kΩ cm^{-1} (σ = 26 ± 8 S m^{-1}) for GGp.

The electro-mechanical response of lines printed on LDPE showed that they completely fail and no longer conduct at a much smaller strain (< 6%) than the substrate (~100%) could withstand (**Figure 6**a). In contrast, the printed lines on GGp

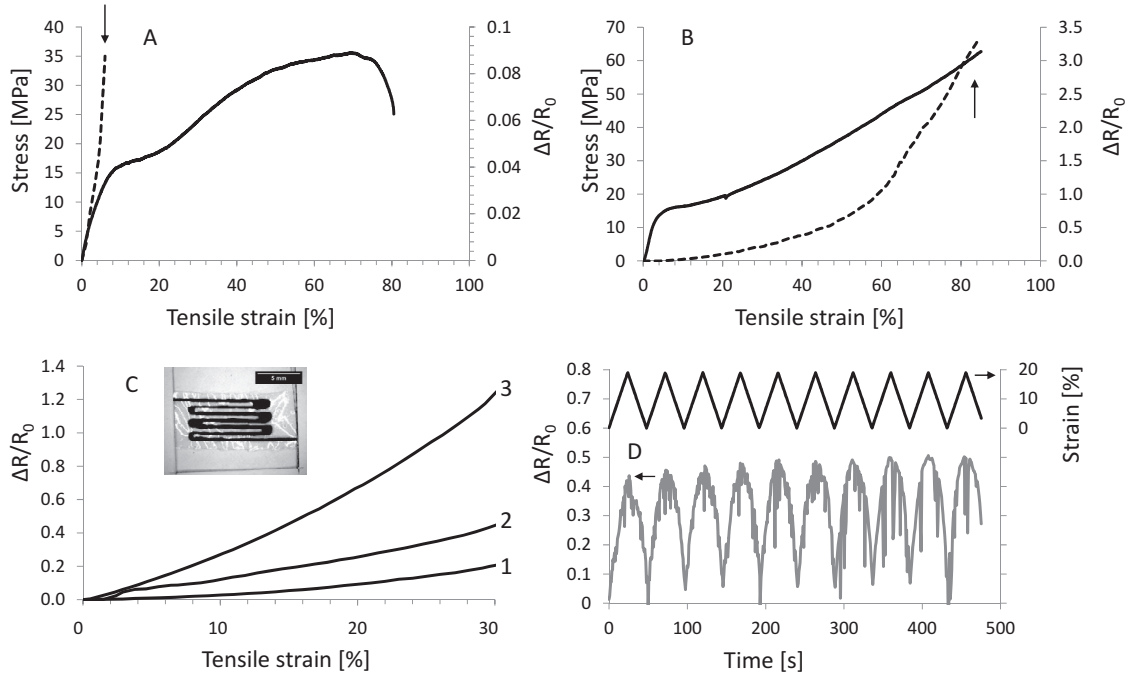

Figure 6. The stress and fractional resistance ($\Delta R/R_0$) as a function of tensile strain for NTI lines (1 layer) printed onto a) LDPE and b) CHp substrates. Arrows in (a,b) indicate the strain at which the printed lines electrically fail. c) Fractional resistance as function of strain for straight line gauges consisting of 1 (line 1) and 6 (line 2) printed layers and uniaxial strain gauge (line 3) geometries. Inset: optical microscopy image of uniaxial strain gauge. d) Fractional resistance and strain as a function of time for straight line gauges (10 layers) printed on textile substrate.

Table 2. Summary of mechanical and electrical properties of substrates and substrates with printed lines. Conductivity, Young's modulus, tensile strength, strain-at-failure, and work of extension are indicated by σ, E, TS, γ, and U_E, respectively. Material 1 is a free-standing film prepared by evaporative casting of NTI ink, which is composed of gellan gum (6.67 mg mL^{-1})–MWNT (3.3 mg mL^{-1}). Material 2 is a free-standing film consisting of commercial LDPE, materials 4 and 6 are free-standing films prepared by evaporative casting of plasticized gellan gum (GGp) and chitosan (CHp) solutions. Materials 3, 5 and 7 are prepared by printing the NTI ink onto glass, LDPE, GGp and CHp substrates, respectively.

Material	Substrate	Ink	σ [S m^{-1}]	E [MPa]	TS [MPa]	γ [%]	U_E [MJ m^{-3}]
1	–	NTI	2532 ± 66	3079 ± 756	8.5 ± 0.1	2.3 ± 1.5	0.55 ± 0.48
2	LDPE	–	–	0.239 ± 0.004	8.5 ± 0.1	103 ± 33	8.2 ± 2.7
3	LDPE	NTI	1914 ± 172	0.310 ± 0.036	36.1 ± 1.5	82 ± 2	21.4 ± 0.4
4	GGp	–	–	1486 ± 94	100 ± 5	17 ± 4	11.6 ± 3.8
5	GGp	NTI	26 ± 8	1133 ± 105	73 ± 14	15 ± 5	7.2 ± 3.5
6	CHp	–	–	777 ± 195	46.8 ± 4.8	64 ± 6	17.2 ± 2.6
7	CHp	NTI	107 ± 23	595 ± 148	53 ± 10	70 ± 15	21.1 ± 6.7

and CHp electrically fail at the same strain values at which the substrate fractured, i.e., 15% and 70%, respectively (Figure 6b, **Table 2**). Films prepared by evaporative casting of the ink solution fail at strain values of ~2% (see Table 2). As such, absorption into a flexible, miscible matrix can mitigate the intrinsic brittleness of the conducting ink. This suggests that absorption may provide some mechanical advantages for flexible conductors, to offset its disadvantage to the electrical characteristics due to interaction with the substrate.

Optical and scanning electron microscopy was used to explore the surface morphology of printed NTI lines on CHp substrate before and after straining to failure. In unstrained samples, the surface was found to consist of smooth, aligned ridges (Figure 5b); likely produced through the ink filament drying in a similar manner to coffee upon paper (wherein the hydrophilic, absorbing substrate fixes the contact line of the liquid during evaporation, resulting in varying deposition of material along the drop radius or filament width).[42] Following strain to failure (70%), the surface was found to be "cobblestoned", with the aligned ridges crossed by surface cracks at which the MWNTs were found to be pulled cleanly out of the matrix (Figure 5c–f). At the fracture surface, a discrete interface between the conducting line and the insulating substrate could be confirmed, and more fiber pull-out was resolved.

2.5. Strain Gauge and Actuation Behavior

The electrical and mechanical behavior of NTI printed onto CHp (NTI-CHp) was found to have some interesting nuances. Unlike GGp, a slight improvement of the extensibility and toughness was noted over the substrate, which could be further increased by printing multiple lines or multiple layers (i.e., failure strain of 90 ± 10% in a 6-layered composite). The same effect was not observed upon printing a gellan gum ink (prepared in the same fashion as the NTI ink but without the addition of carbon nanotubes) onto CHp. Furthermore, printing multiple layers of the NTI ink on CHp resulted in a decrease in the resistance from 30 ± 10 κΩ cm^{-1} (1 layer) to 4.2 ± 0.9 kΩ cm^{-1} (6 layers).

Strain-gauging is based on relating changes in the resistance to changes in the strain, with strain sensitivity determined by the magnitude of the resistance or strain change. The resistance change is commonly related to the strain through the strain sensitivity gauge factor (*GF*) defined as:

$$GF = \frac{\Delta R / R_0}{\varepsilon} \quad (3)$$

where $\Delta R/R_0$ and ε indicate the fractional resistance and strain, respectively. It is evident from Figure 6a that the strain sensitivity for NTI-LDPE is modest, i.e., GF = 0.5 (0–6% strain). Figure 6b shows that the strain-dependent resistance of NTI-CHp exhibits 2 distinct regions separated by a significant change in the slope around 60% strain. Each of these regions can be used to obtain a GF value. Regression analysis shows that the first region exhibits a GF value of 1.0 ± 0.2, i.e., $\Delta R/R_0$ = 30% at 30% strain. It was found that printing additional layers could result in an improvement of the GF value. For example, printing 6 layers instead of 1 improved the GF value from 1.0 ± 0.2 to 1.4 ± 0.1 (Figure 6c). Alternatively, the first distinctive region is defined as a pre-strain gauge treatment, and the GF can be calculated after adjusting the strain and $\Delta R/R_0$ for this treatment. This is a commonly used practice employed to enhance the mechanical and electrical characteristics of fibers.[43–45] This results in an improvement of the GF value for 1 printed layer from 1.0 ± 0.2 to 2.8 ± 0.2 in the second region, which after adjustment (for pre-strain treatment) corresponds to a strain range of 0–40%. Similar improvements can be achieved for a track consisting of 6 printed lines resulting in a GF improvement from 1.4 ± 0.2 to 14.6 ± 0.5 (pre-strain treatment of 45%, adjusted strain range 0–20%).

Strain gauges are commonly used in mechanical analysis to evaluate the stress state of a material or technology during use. Traditional metal foil strain gauges (constantin or nickel-chromium alloy) are limited in their strain region (0–5%), their strain sensitivity (gauge factor 2.0–3.2), and their application to a surface (adhesive). Carbon nanotube containing strain gauges have been demonstrated using fabrication methods such as melt processing (GF of 7 over 1% strain), dyeing (GF of 1 over 50% strain) and mixing (GF of 6 over 1% strain).[46–48] Recently, gauges with low strain sensitivity (GF of 0.06) capable of measuring high strain (150%) with high durability (10 000 cycles) were fabricated using a multi-step film transfer process.[49] The fabrication of these gauges involved manual assembly of

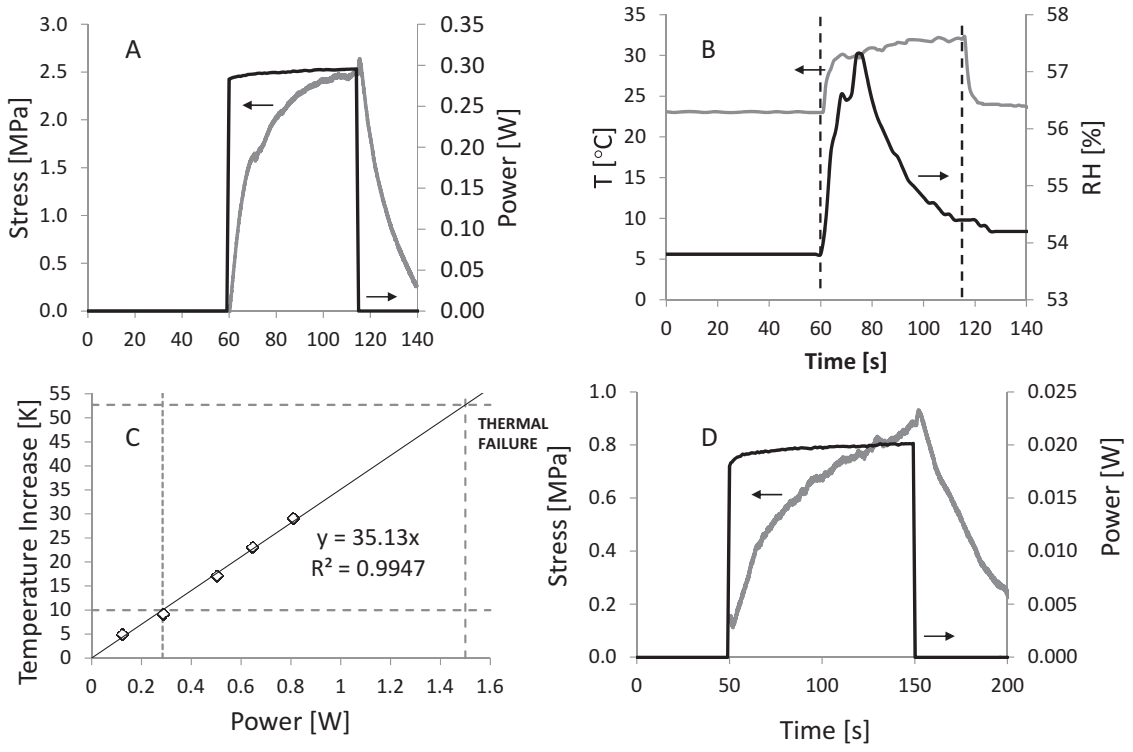

Figure 7. a) Stress of contraction and electrical power consumption and b) temperature and adjacent relative humidity (RH) for a MWNT composite (M_f = 0.31) film over time under the application of 6 V (between 60 and 115 s). c) Increase in MWNT composite (M_f = 0.31) film temperature from 21 °C (ΔT) as a function of electrical power consumption. d) Stress of contraction and electrical power consumption for a NTI line (6 layers) printed onto a CHp substrate over time under the application of 10V (between 50 and 150 s). All measurements were carried out under controlled ambient conditions (21 °C, 50% RH). Stress for printed materials is evaluated using cross-section of the substrate + printed line.

aligned chemical vapour deposition grown CNT films on a flexible substrate (poly(dimethylsiloxane)).[49] In this context, a printing process as described in this paper offers flexibility to both the geometry and the application of the gauge material to a substrate. This was demonstrated by printing a uniaxial strain gauge (6 layers, resistance = 4.2 kΩ cm^{-1}) upon a CHp substrate. Regression analysis showed that the gauge factor was found to be considerably amplified over a straight line by the strain gauge geometry, i.e., an increase in GF value from 1.4 ± 0.2 to = 4.2 ± 0.1 (Figure 6c).

Thus, printed NTI structures on CHp are able to function as sacrificial strain sensors with GF values ranging between 1.0 and 14.6. A repeatable electrical response to strain cycling was also easily obtained by printing the NTI upon a spandex-composite textile material (10 printed layers, resistance = 40 kΩ cm^{-1}). Over 10 strain-relaxation cycles the printed structure exhibited a GF value of 2.2 ± 0.1, with negligible differences between the GF values of the strain and relaxation parts of each cycle (Figure 6d).

Joule heating, a phenomenon that is seldom considered helpful, was unexpectedly found to enable the GG-MWNT dry structures to actuate when given sufficient electrical power. During mechanical testing, it was observed that passing a current through films under tension produced considerable stress. A composite, constructed using GG-MWNT film (M_f = 0.31) and double sided tape (with electrical contacts provided by silver paint), was found to significantly and repeatedly flex. Flexure required 0.4W of electrical power, with the rate of contraction under voltage roughly twice the rate of expansion out of voltage (Figure S5, Supporting Information). Indirect monitoring the temperature of the films and the relative humidity near the films showed a correlation between a peak in the film temperature, the adjacent relative humidity (RH), the film stress and the current (**Figure 7**a,b). This correlation suggests the role of Joule heating in the actuation, whereby heat generated at higher currents through the resistors removes some of the moisture content from the hygroscopic GG matrix. This causes a volume contraction and the evolution of stress and strain when the composite is constrained. The peak temperature was found to scale linearly with the electrical power consumption, until the thermal degradation of the matrix (Figure 7c).

Cycling of the films was found to be mostly inhibited by the expansion rate, which was in turn related to the ambient humidity. Supplying more power markedly increased the rate of contraction, but only if sufficient time was given for the film to recover its moisture following the previous cycle. Cycles with higher power–and higher temperatures–required longer recovery times, slowing the cycle frequency. The actuating material was found to be able to contract against significant tensile loads (i.e., ~5 MPa), and in a repeatable manner under different loading situations and frequencies.

A composite structure formed from printing 6-layers of the NTI ink upon a CHp substrate was able to generate a contractive stress of 0.93 MPa when drawing ~20 mW of power over

100 s (Figure 7d). The average electrical energy needed to generate 1 MPa of contractive stress for these printed materials was found to be 2.0 ± 0.5 J. In comparison, GG-MWNT (M_f = 0.31) films were able to generate larger amounts of contractive stress than the printed materials, but at an increased cost in electrical energy consumption. These films required 16 J in electrical energy (300 mW of power over 55 s) to generate 2.6 MPa of contractive stress. This indicates that the actuators prepared by evaporative casting required about 2.5 times the amount of electrical energy (5.2 ± 1.3 J) to generate the same amount of contractive stress as the printed actuators. The power-mass density of the GG-MWNT material was estimated at 2 W kg^{-1}, which is comparable to other Joule heating actuators.[50]

3. Conclusions

The dispersion of multiwalled carbon nanotubes into gellan gum, solutions was optimized with respect to the minimum dispersant:MWNT ratio, which was then used to scale up the CNT concentration. The resulting dispersions were further optimized by thickening with gellan gum to facilitate extrusion printing of conducting nanotube networks.

It was shown that gellan gum is able to sustain high concentrations of dispersed MWNTs, enabling the preparation of composite materials with high CNT loading fraction (>30% by weight) by evaporative casting. These composites exhibited a conductivity value (5030 S m^{-1}) close to the maximum achievable value with this type of MWNTs. Tensile testing showed that these nanotubes are able to mechanically reinforce GG at low loadings, but significantly embrittle GG at higher loadings.

The printed nanotube networks (on absorbing flexible substrates) had interesting mechanical and electrical characteristics which were used to demonstrate their applicability as strain gauges and actuators. The interaction between ink and absorbing substrates provided mechanical advantages (order of magnitude increase in ductility), at a cost of electrical conductivity (increase in resistance) compared to films prepared by evaporative casting. Gauge factors ranged from GF = 1.4 for a straight line geometry to GF = 4.2 for a uniaxial strain gauge over 20% strain. Higher GF values were achievable by pre-strain treatment, i.e., GF = 14.2 over a comparable strain region. MWNTs were found to impart actuation ability to both bulk and printed networks through Joule heating and the evaporation of water content from the hygroscopic GG matrix. Printed materials consumed about 2.5 times less energy to generate the same amount of contractive stress compared to bulk networks prepared by evaporative casting.

4. Experimental Section

Materials: Multiwalled carbon nanotubes (MWNTs), produced using catalytic chemical vapor deposition were purchased from Nanocyl (3100, batch # 100825, see Supporting Information for details on level of graphitization, length and diameter). Low-acyl gellan gum (GG), with a molecular weight range of 2–3 × 10^5 Da and ~100% deacylation, was gifted by CP Kelco (Gelzan CM, Lot # 9K6968A). Chitosan (CH), with a molecular weight range of 1.9–3.1 × 10^5 Da and >79% deacylation, was purchased from Aldrich (medium molecular weight, batch #MKBB0566). Glycerol (99.5%) was purchased from Sigma-Aldrich (G7043, batch #033K0097). Low density polyethylene (LDPE) thin films were sampled from consumer cling wrap (Glad; Woolworths). Polytetrafluoroethylene (PTFE) thin films were obtained from Advanced Gaskets and Supplies Wollongong. Photopaper (Kodak Premium, 200 g/m^2, matte coating) and glass slides (J. Melvin Freed 301M) were used as received. 20% spandex–30% nylon–50% wool/cellulose acetate composite textiles were purchased from Dunnes Stores (Ireland). All solutions were produced using Milli-Q water (resistivity = 18.2 MΩ cm).

Ink Formulation: GG stock polymer solutions were prepared by adding ≥2 wt% solid to hot water (80 °C) and mixing at temperature for a minimum of 2 hours (Stuart CB162 magnetic stirrer/hot plate). The stock solution was volumetrically diluted into the required concentrations through hot pipetting (60 °C), and mixed under high shear (IKA Vortex Genius 3).

MWNTs were mixed with diluted GG polymer solutions and dispersed through ultrasonication (Branston 450 Digital Sonifier) under mild conditions (6 W or 0.36 kJ min^{-1}, at a horn frequency of 19.850–20.050 kHz, pulsed for 0.5 s on/off). Energy was delivered using a microtip horn (Titanium, 3 mm diameter, Consonic) to a sample volume of 9 mL cooled to 6 ± 1 °C. The dispersions were monitored through taking thief samples (50 µL) at varying time intervals, of which 10 µL was diluted to measure the UV-Vis absorbance spectrum (Varian Cary 500 Scan UV-VIS-NIR spectrophotometer). An additional 10 µL of the thief sample was plated between glass slides (75 × 25 mm^2) and used to check for visible agglomerates using optical microscopy (Leica Z16APO Digital Macroscope). A standard curve was constructed through diluting a 5 mg mL^{-1} GG, 5 mg mL^{-1} MWNT high quality dispersion and measuring the absorbance at 600 nm as a function of MWNT concentration. All MWNT solutions were diluted to a similar concentration range (0 – 6.67 ppm MWNT).

Thickening involved volumetrically diluting MWNT dispersions with concentrated GG stock solutions and Milli-Q water. Dispersions were mixed under high shear and then degassed under bath sonication (Unisonics XFP4). All steps were undertaken at 60 °C.

Substrate and Film Preparation: Plasticized CH (CHp) free-standing films were prepared using solutions of 20 mg mL^{-1} solid CH, 6 mg mL^{-1} glycerol dissolved into 1 wt% acetic acid over 4 hours at 80 °C. 150 mL of the solution was cast into a 28.5 × 23.0 cm^2 poly(methyl methacrylate) tray, and evaporated overnight inside a controlled temperature and humidity chamber (Thermoline 150, set at 21 °C and 50% relative humidity, RH) equivalent to an evaporation rate of 20 µL cm^{-2} h^{-1}). Plasticized GG (GGp) films were prepared following similar steps, but substituting the CH for the GG and the acetic acid for Milli-Q water.

Dry ink films were produced through casting 5 mL of the ink into a 5.6 cm diameter PET petri dish, and evaporating the ink into a free-standing film inside the controlled temperature and humidity chamber (21 °C, 50% RH).

Extrusion Printing: GG-MWNT inks were extruded onto substrates using a custom-built syringe printer.[7] The printing parameters (syringe tip diameter, the ink flow-rate/pressure, and the substrate feed rate) were optimized for a given ink to deliver repeatable, unbroken and unblotted lines at the highest possible resolution. The MWNT ink developed in this work was delivered to a range of substrates at a flow rate of 15 µL min^{-1} (35 kPa) through a 50 µm radius tip onto a substrate moving at 450 mm min^{-1}. This results in a deposition rate of 40 nL mm^{-1}. Following printing, the substrates were dried and conditioned under controlled temperature and humidity (21 °C, 50% RH).

Electrical Characterization: Films were prepared for electrical characterization through sectioning them into thin strips (typically 4 × 30 mm^2), measuring their thickness (Mituyo digital micrometer), width (optical microscope), and mounting them onto glass slides (using double sided tape). Low resistance contacts of a desired channel length were prepared on the film surface using silver paint (Spi-paint 05002-AB) and copper tape (3M #1181 electrical tape). Contacts were placed under compression (approximately 10^5 Pa) using bull-clips (isolated by glass slides) prior to measurement.

An arbitrary waveform generator (Agilent 33220A) was used to apply a step-wise DC-voltage ramp to a prepared sample over a known conducting channel length (L). The current (I) and the voltage (V) response were measured using a digital multimeter (Agilent 34410A). Measurements were repeated for a minimum of four channel lengths, over four films. Electrical resistance and conductivity values were evaluated as described in the Supporting Information. The temperature and humidity during electrical testing was logged using a computer controlled data-logger (Jaycar, Digitech QP-6013).

Mechanical Characterization: The mechanical properties of the substrates and printed composites were determined under tension using the Shimadzu EZ-S Universal Mechanical Tester (50N load cell, 500N capacity screw-type flat grips, sampling at 20 Hz), with 24×4 mm^2 thin film samples (gauge length 15 mm) strained to failure at a strain rate of 1% s^{-1}. Thin film samples were mounted to paper windows using double sided tape, which were cut prior to testing. The thickness and width of each sample was measured at five points along the gauge length prior to testing (Mituyo digital micrometer, and the microscope). Tests were repeated a minimum of three times, under the same conditions as the current-voltage measurements. Stress and strain were calculated using the average cross-sectional area and the measured gauge length. The elastic modulus, ultimate tensile stress, extension of failure, and work of extension was calculated for each sample using the gradient of the linear part of the stress-strain curve, the maximum stress, the failure strain and the area under the stress-strain curve, respectively.

Measuring stress relaxation in CHp and GGp substrates involved straining CHp samples to 7% strain at 10% s^{-1} strain rate, and GGp samples to 3.5% strain at 2% s^{-1} strain rate. The force was monitored for 100 s following the strain step.

Electro-Mechanical Characterization: The electrical response under strain was measured by contacting the mounted films and printed composites on either side of the gauge length, applying a DC voltage (<10V, Agilent 33220A), and sampling the current (0.5 Hz, min 10 µA, Agilent 34410A) as the sample was strained. The current was passed through the sample for a minimum of 5 minutes prior to testing, to allow the sample to equilibrate relative to Joule heating.

The actuation response to voltage in printed composites and thin films was measured by mounting the film within the mechanical tester, pre-straining the material (0.1%), and measuring the force (at 20 Hz, Shimadzu EZ-S) and current (at 0.5 Hz, Agilent Agilent 34410A) over time as a function of applied DC voltage (≤10V, Agilent 33220A). A non-contact infrared (IR) thermometer (Digitech QM-7221, emissivity set to 0.99, 4 mm sampling area, 1 Hz sampling rate) and a data logger (Digitech QP-6013, 0.5 Hz sampling rate) were used to monitor both the thin film temperature and surface humidity during the actuation response.

The strain response could be directly observed through constructing a sandwich composite of double sided tape, ink thin film ($38 \times 5.5 \times 0.018$ mm^3), and silver paint (flexible contact), and applying a DC-voltage (≤10V, Agilent 33220A) whilst the composite was vertically suspended. Video during the strain cycles was taken using a digital microscope (Dinolite AM-211; 15 frames per second). Frames were analysed to determine the maximum deflection using the ImageJ software (freely available from the National Institutes of Health, USA).[51]

Thermogravimetric Analysis: Thermogravimetric measurements were obtained using a thermal analyzer (Shimadzu TGA). Film samples were analysed at a heating rate of 10 °C/min under a N_2 flow rate of 50 mL/min.

Rheology: The rheology of 600 µL ink samples was characterized using a controlled shear strain rheometer (Anton Paar Physica MCR-301) with a cone and plate measuring system (49.972 mm diameter, 0.992° angle, 97 µm truncation) and a heat controlled sample stage (Julabo Compact Recirculating Cooler AWC 100). The viscosity was measured as a function of shear rate (1–50 s^{-1}). The temperature dependence in the viscosity (at 20 s^{-1} shear rate) was measured using a heating and cooling rate of 5 °C min^{-1}.

Contact Angle: Contact angles were measured using a goniometer (Dataphysics Contact Angle System OCA), with axisymmetric drop shape analysis carried out using the SCA 20 software. Ink-substrate contact angles were obtained through suspending 5 µL drops of the NTI ink upon a 300 µm diameter tip, bringing the tip in contact with the substrate, and withdrawing the tip, leaving the droplet to spread upon the substrate. All measurements were taken at 24 ± 0.5 °C, 60% RH, with ambient light dimmed to improve contrast.

Optical and Electron Microscopy: The surface features, cross-sectional morphology and fracture surfaces of the printed composites were investigated through low and high magnification optical microscopy (Leica Z16APO Digital Macroscope) and scanning electron microscopy (JEOL JSM7500FA cold Field Emission Gun Scanning Electron Microscope).

Statistical Treatment: The reported results are averages of the values obtained. Reported numerical errors and graphical error bars are given as ± 1 standard deviation (SD). Data and outliers were rejected either when instrumental error was known to have occurred, or if data failed a Q-test with a confidence interval ≥95%.

Supporting Information

Supporting Information is available from the Wiley Online Library or from the author.

Acknowledgements

This work was supported by Australian Research Council (ARC) Centre of Excellence Program, ARC Future Fellowship (M.P.) and University of Wollongong. Dr. Tony Romeo is thanked for assistance with electron microscopy. The authors thank Profs. Geoff Spinks, Paul Calvert, Hugh Brown, and Drs. Phil Whitten and Ross Clark for useful discussions.

Received: March 15, 2012
Revised: May 10, 2012
Published online: July 6, 2012

[1] A. C. Siegel, S. T. Phillips, M. D. Dickey, N. Lu, Z. Suo, G. M. Whitesides, *Adv. Funct. Mater.* **2010**, *20*, 28.
[2] J. A. Rogers, T. Someya, Y. Huang, *Science* **2010**, *327*, 1603.
[3] T. Yamada, Y. Hayamizu, Y. Yamamoto, Y. Yomogida, A. Izadi-Najafabadi, D. N. Futaba, K. Hata, *Nat. Nanotechnol.* **2011**, *6*, 296.
[4] J. A. Lewis, *Mater. Today* **2004**, *7*, 32.
[5] P. Calvert, R. Crockett, *Chem. Mater.* **1997**, *9*, 650.
[6] P. Calvert, T. L. Lin, H. Martin, *High Perform. Polym.* **1997**, *9*, 449.
[7] C. A. Mire, A. Agrawal, G. G. Wallace, P. Calvert, M. in het Panhuis, *J. Mater. Chem.* **2011**, *21*, 2671.
[8] P. Calvert, *Chem. Mater.* **2001**, *13*, 3299.
[9] M. Singh, H. M. Haverinen, P. Dhagat, G. E. Jabbour, *Adv. Mater.* **2010**, *22*, 673.
[10] S. Iijima, *Nature* **1991**, *354*, 56.
[11] P. M. Ajayan, *Chem. Rev.* **1999**, *99*, 1787.
[12] R. H. Baughman, A. A. Zakhidov, W. A. de Heer, *Science* **2002**, 787.
[13] M. in het Panhuis, *J. Mater. Chem.* **2006**, *16*, 3598.
[14] A. V. Kyrylyuk, P. van der Schoot, *Proc. Nat. Acad. Sci. USA* **2008**, *105*, 8221.
[15] D. Stauffer, A. Aharony, *Introduction to Percolation Theory*, CRC Press, Florence, KY **1994**.
[16] W. Bauhofer, J. Z. Kovacs, *Compos. Sci. Technol.* **2009**, *69*, 1486–1498.
[17] S. B. Kharchenko, J. F. Douglas, J Obrzut, E. A. Grulke, K. B. Migler, *Nat. Mater.* **2004**, *3*, 564.

[18] Y. Y. Huang, S. V. Ahir, E. M. Terentjev, *Phys. Rev. B* **2006**, *73*, 125422.
[19] L. A. Girifalco, M. Hodak, R. S. Lee, *Phys. Rev. B* **2000**, *62*, 13104.
[20] F. Lu, L. Gu, M. J. Meziani, X. Wang, P. G. Luo, L. Monica Veca, L. Cao, Y. P. Sun *Adv. Mater.* **2009**, *21*, 139.
[21] J. Boge, L. Sweetman, M. in het Panhuis, S. F. Ralph, *J. Mater. Chem.* **2009**, *19*, 9131.
[22] H. Wang, *Curr. Opin. Colloid Interface Sci.* **2009**, *14*, 364.
[23] V. C. Moore, M. S. Strano, E. H. Haroz, R. H. Hauge, R. E. Smalley, J. Schmidt, Y. Talmon, *Nano Lett.* **2003**, *3*, 1379.
[24] M. S. Strano, V. C. Moore, M. K. Miller, M. J. Allen, E. H. Haroz, C. Kittrell, R. H. Hauge, R. E. Smalley, *J. Nanosci. Nanotechnol.* **2003**, *3*, 81.
[25] A. J. Blanch, C. E. Lenehan, J. S. Quinton, *Carbon* **2011**, *49*, 5213.
[26] A. Lucas, C. Zakri, M. Maugey, M. Pasquali, P. van der Schoot, P. Poulin, *J. Phys. Chem. C* **2009**, *113*, 20599.
[27] J. R. Yu, N. Grossiord, C. E. Koning, J. Loos, *Carbon* **2007**, *45*, 618.
[28] I. Giavasis, L. M. Harvey, B. McNeil, *Crit. Rev. Biotechnol.* **2000**, *20*, 177.
[29] E. Miyoshi, K. Nishinari, *Colloid Polym. Sci.* **1999**, *734*, 727.
[30] M. F. Islam, E. Rojas, D. M. Bergey, A. T. Johnson, A. G. Yodh, *Nano Lett.* **2003**, *3*, 269.
[31] J. N. Coleman, A. Fleming, S. Maier, S. O'Flaherty, A. I. Minett, M. S. Ferreira, S. Hutzler, W. J. Blay, *J. Phys. Chem. B* **2004**, *108*, 3446.
[32] M. Tako, T. Teruya, Y. Tamaki, T. Konishi, *Colloid Polym. Sci.* **2009**, *287*, 1445.
[33] G. J. Heymach, D. E. Jost, *J. Polym. Sci. Part C* **1968**, *153*, 145.
[34] M. L. Tsaih, R. H. Chen, *Polymer* **2003**, *90*, 3526.
[35] A. J. Granero, J. M. Razal, G. G. Wallace, M. in het Panhuis, *Adv. Funct. Mater.* **2008**, *18*, 3759.
[36] A. Aldalbahi, M. in het Panhuis, *Carbon* **2012**, *50*, 1197.
[37] T. C. Mezger, *The Rheology Handbook*, Vincentz Network, Hannover, Germany **2006**.
[38] I. C. Alupei, M. Popa, A. Bejenariu, S. Vasiliu, V. Alupei, *Eur. Polym. J.* **2006**, *42*, 908.
[39] N. Barbani, M. L. Coluccio, C. Cristallini, G. D. Guerra, E. Rosellini, *J. Appl. Polym. Sci.* **2010**, *118*, 3131.
[40] M. T. Byrne, Y. K. Gun'ko, *Adv. Mater.* **2010**, *22*, 1672.
[41] M. Cadek, J. N. Coleman, K. P. Ryan, V. Nicolosi, G. Bister, A. Fonseca, J. B. Nagy, K. Szostak, F. Béguin, W. J. Blau, *Nano Lett.* **2004**, *4*, 353.
[42] W. R. Small, C. D. Walton, J. Loos, M. in het Panhuis, *J. Phys. Chem. B* **2006**, *110*, 13029.
[43] A. J. Granero, P. Wagner, K. Wagner, J. M. Razal, G. G. Wallace, M. in het Panhuis, *Adv. Funct. Mater* **2011**, *21*, 955.
[44] E. Smela, W. Lu, B. R. Mattes, *Synth. Met.* **2005**, *151*, 25.
[45] G. M. Spinks, V. Mottaghitalab, M. Bahrami-Saniami, P. G. Whitten, G. G. Wallace, *Adv. Mater.* **2006**, *18*, 637.
[46] W. Zhang, J. Suhr, N. Koratkar, *J. Nanosci. Nanotechnol.* **2006**, *6*, 960.
[47] M. in het Panhuis, J. Wu, S. A. Ashraf, G. G. Wallace, *Synth. Met.* **2007**, *157*, 358.
[48] G. T. Pham, Y. B. Park, Z. Liang, C. Zhang, B. Wang, *Composites Part B* **2008**, *39*, 209.
[49] T. Yamada, Y. Hayamizu, Y. Yamamoto, Y.Yomogida, A. Izadi-Najafabadi, D. N. Futaba, K. Hata, *Nat. Nanotechnol.* **2011**, *6*, 296.
[50] H. Okuzaki, K. Funasaka, *J. Intell. Mater. Sys. Struct.* **1999**, *10*, 465.
[51] W. Rasband, *Image J*, **2011**, http://imagej.nih.gov/ij (accessed June 2011).